Materials Science & Engineering C 124 (2021) 112079

Contents lists available at ScienceDirect

Materials Science & Engineering C

journal homepage: www.elsevier.com/locate/msec

An organic-inorganic hybrid scaffold with honeycomb-like structures enabled by one-step self-assembly-driven electrospinning

Yaping Ding [a,*], Wei Li [a], Dirk W. Schubert [b], Aldo R. Boccaccini [c], Judith A. Roether [b,*], Hélder A. Santos [a,d,**]

[a] Drug Research Program, Division of Pharmaceutical Chemistry and Technology, Faculty of Pharmacy, University of Helsinki, FI-00014 Helsinki, Finland
[b] Institute of Polymer Materials, University of Erlangen-Nuremberg, Martensstrasse 7, 91058 Erlangen, Germany
[c] Institute of Biomaterials, University of Erlangen-Nuremberg, Cauerstrasse 6, 91058 Erlangen, Germany
[d] Helsinki Institute of Life Science (HiLIFE), University of Helsinki, FI-00014 Helsinki, Finland

ARTICLE INFO

Keywords:
Organic-inorganic hybrid scaffolds
Electrospinning
Self-assembly
Honeycomb-like architecture

ABSTRACT

Electrospun organic/inorganic hybrid scaffolds have been appealing in tissue regeneration owing to the integrated physicochemical and biological performances. However, the conventional electrospun scaffolds with non-woven structures usually failed to enable deep cell infiltration due to the densely stacked layers among the fibers. Herein, through self-assembly-driven electrospinning, a polyhydroxybutyrate/poly(ε-caprolactone)/58S sol-gel bioactive glass (PHB/PCL/58S) hybrid scaffold with honeycomb-like structures was prepared by manipulating the solution composition and concentration during a one-step electrospinning process. The mechanisms enabling the formation of self-assembled honeycomb-like structures were investigated through comparative studies using Fourier-transform infrared spectroscopy (FTIR), differential scanning calorimetry (DSC) and thermogravimetric analysis (TGA) between PHB/PCL/58S and PHB/PCL/sol-gel silica systems. The obtained honeycomb-like structure was built up from nanofibers with an average diameter of 370 nm and showed a bimodal distribution of pores: large polygonal pores up to hundreds of micrometers within the honeycomb-cells and irregular pores among the nanofibers ranging around few micrometers. The cell-materials interactions were further studied by culturing MG-63 osteoblast-like cells for 7 days. Cell viability, cell morphology and cell infiltration were comparatively investigated as well. While cells merely proliferated on the surface of non-woven structures, MG-63 cells showed extensive proliferation and deep infiltration up to 100–200 μm into the honeycomb-like structure. Moreover, the cellular spatial organization was readily regulated by the honeycomb-like pattern as well. Overall, the newly obtained hybrid scaffold may integrate the enhanced osteogenicity originating from the bioactive components, and the improved cell-material interactions brought by the honeycomb-like structure, making the new scaffold a promising candidate for tissue regeneration.

1. Introduction

Tissue engineering has emerged as a multidisciplinary approach involving the principles of biology and engineering to replace or restore the diseased or lost tissue or organs [1]. To mimic the dynamics of biological microenvironment for cells, three-dimensional (3D) porous scaffolds with tunable pore sizes are designed to accommodate cells and support cell adhesion, proliferation, infiltration, and other metabolism behaviors [2]. One of the challenges is to fabricate biomimetic scaffolds to resemble the complex extracellular matrix (ECM) which consists of fibrous protein networks [3]. Electrospun scaffolds comprised of continuous micro/nano-fibers with non-woven structures are considered as superior candidates to mimic ECM, owing to the ultra-thin fiber diameter and high porosity, although the densely packed layer-by-layer structure impedes their wide applications [4–6]. The pore size, pore shape, and porous interconnections can highly influence the adhesion, proliferation, and deep infiltration of cells into the fibrous scaffolds and circulation of metabolites and nutrients [7]. The relative small pore size of electrospun fibermats due to the close fiber deposition hinders the sufficient cell infiltration and following cell ingrowth [8].

* Corresponding authors.
** Correspondence to: H.A. Santos, Faculty of Pharmacy and Helsinki Institute of Life Science (HiLIFE), University of Helsinki, FI-00014 Helsinki, Finland.
E-mail addresses: yaping.ding@helsinki.fi (Y. Ding), judith.roether@fau.de (J.A. Roether), helder.santos@helsinki.fi (H.A. Santos).

https://doi.org/10.1016/j.msec.2021.112079
Received 25 January 2021; Received in revised form 21 March 2021; Accepted 23 March 2021
Available online 27 March 2021

Among all the techniques to enlarge the pore size of electrospun scaffolds, the self-assembly-driven electrospinning (SAES) offers a new perspective for electrospun 3D scaffolds [9]. By manipulating the parameters, such as solution concentration, applied voltage, and collectors, honeycomb-like nanofibrous structures that were built-up by polygonal pores with in-depth walls, consisting of conglutinated and uniaxially aligned nanofibers, can be prepared through the self-assembly process of nanofibers [9–13]. The size of the polygonal pores can be increased to over 200 μm with the depth of over 150 μm [10]. As a hierarchy architecture that can integrate both macro-and micropores, the electrospun scaffold with honeycomb-like structures will be potentially very promising in tissue engineering, such as the regeneration of cardiac tissue, bone, skin, and cartilage [14–17]. As a typical example for bone tissue engineering, it can mimic the ECM and the inner spongy structure of the bone tissue [18–19].

Except for the structural features, material compositions also play crucial roles in the scaffolds fabrication process and meanwhile endow critical functions to the scaffolds. As electrospun scaffolds, pure polymer structures may be incompetent in tissue regeneration, whereas a second inorganic component could add complementary functions to the scaffolds, such as osteogenicity for bone tissue regeneration, antibacterial activity and angiogenesis for wound healing, and electrical conductivity and antioxidant property for nerve repair [20–22]. Honeycomb-like architectures have been prepared through the one-step SAES approach from pure polymers, such as polyacrylonitrile, polyvinyl alcohol and poly (ε-caprolactone) (PCL), on both conducting and insulating substrates [9–10,12]. However, as far as we know, there has been no study on whether the honeycomb-like structure can be achieved from organic-inorganic hybrids through this SAES approach, which will be the interest of this study. The addition of inorganic components may complicate the optimization process since the overall properties of polymer solutions could have been altered and more variables are introduced to the system.

In our previous study, prepared by combinational sol-gel method and electrospinning technique, polyhydroxybutyrate/poly-ε-caprolactone/58S sol-gel derived bioactive glass (PHB/PCL/58S) hybrid scaffolds (from the solution at a concentration of 5% w/v, named as 5%P5B1), which balanced the rigidity of PHB, the ductility of PCL and the bioactivity of 58S bioactive glass, were demonstrated to show favorable biocompatibility and high osteogenicity [23]. 5%P5B1 hybrid scaffolds are non-woven fibermats consisting of random microfibers with an average diameter of 1.2 μm and small pores in the range of few micrometers [23]. Taking this optimized hybrid system as an example, here we aim to investigate how to achieve honeycomb-like structures from organic-inorganic hybrids through the SAES approach and what could be the influencing factors. Cell-scaffolds interactions were further studied for comparison purpose. To the best of our knowledge this is the first report on honeycomb-like structures from an organic-inorganic hybrid system prepared through self-assembly-driven electrospinning approach.

2. Experimental

2.1. Materials

Polyhydroxybutyrate (PHB, M_w = 437 kDa) and polycaprolactone (PCL, M_w = 48–90 kDa) were dissolved in chloroform (CF) and *N*, *N*-dimethylformamide (DMF) to prepare the polymer solution. To prepare the 58S bioactive glass sol and the silica sol, tetraethyl orthosilicate (TEOS, 98%), triethyl phosphate (TEP), calcium chloride dihydrate ($CaCl_2 \cdot 2H_2O$), ethanol (EtOH, 99.5%), hydrogen chloride (HCl, 1 N) and DI H_2O were used as precursor, solvent and catalyst. All chemicals were commercially purchased from Sigma-Aldrich.

2.2. Preparation of honeycomb-like hybrid scaffolds

The hybrid scaffolds were prepared through a similar procedure as in our previous study [23]. In short, polymer solutions were prepared by dissolving PHB/PCL (w/w = 7:3) into CF/DMF solvent mixture (v/v = 8:2) at a concentration of 2.5% (w/v) at 70 °C under vigorous stirring. Meanwhile, TEOS, TEP, EtOH, H_2O and $CaCl_2 \cdot 2H_2O$ with the molar ratio of 1: 0.133: 2: 2: 0.6 were mixed and stirred to prepare the 58S sol (mol., 60% SiO_2, 36% CaO, 4% P_2O_5) with an acid catalyst. The sol was first aged at 40 °C for 2 h and then kept at room temperature for 24 h before adding it to the polymer solution.

Afterwards, predetermined amounts of 58S sol were added into the as-prepared PHB/PCL polymer solution to obtain the hybrid solution with an organic/inorganic ratio of 5:1 (2.5%P5B1). A schematic of the preparation process is shown in Fig. 1. Thereafter, the hybrid mixtures were transferred into a 10 ml syringe for electrospinning using the following parameters: flow rate of 4 ml/h, voltage of 15 kV, and working distance of 15 cm. The electrospinning process was always carried out at room temperature (22 ± 2 °C) with the humidity at around 30%–40%. The prepared samples were dried in vacuum oven at 40 °C for 24 h before further characterizations. For comparison purposes, only sol-gel derived silica sol from precursor TEOS was incorporated to the PHB/PCL@CF/DMF solution to prepare a PHB/PCL/silica hybrid scaffold (named 2.5%P5S1) under the same conditions when the solution concentration was reduced to 2.5% (w/v). The preparation process was described in detail in the previous publication [24].

2.3. Physicochemical characterizations

2.3.1. Morphology

The morphologies of the as-prepared samples were observed by scanning electron microscopy (SEM, Ultra Plus, Zeiss, Germany). The accelerating voltage for SEM imaging was 10 kV and all samples were coated with a mixture of gold and palladium before observation. Through SEM images, fiber diameter distributions and (2D) pore size distributions were determined by Image J. The average fiber diameter was calculated based on over 100 fibers, and the pore size distributions were obtained from over 100 pore size readings from SEM images at low magnification of 50×.

2.3.2. Fourier transform infrared spectroscopy

To investigate the chemical structure of obtained samples, attenuated total reflectance Fourier transform infrared spectroscopy (ATR–FTIR, Nicolet 6700, Thermo Scientific) was utilized. For each measurement, 32 spectral scans were repeated in the wavenumber range of 4000–525 cm^{-1}. The spectrum of PHB and PCL mixture at the same ratio was also investigated for comparison purposes.

2.3.3. Wettability

The wettability of the samples was studied by contact angle measurements (CAM 200, KSV, Finland). Three specimens were tested for each composition and five measurements were carried on each specimen. The contact angles were calculated by the software based on the captured images.

2.3.4. Differential scanning calorimetry and thermal gravimetric analysis

The thermal performance was investigated through differential scanning calorimetry (DSC, Q2000, TA Instruments). In the DSC measurements, around 5 mg of each sample was heated from 25 to 200 °C at a rate of 10 °C/min under nitrogen atmosphere. The melting point of the polymers was determined form the melting peaks. Thermogravimetric analysis (TGA, Q5000, TA Instruments) was further conducted from room temperature to 600 °C under nitrogen atmosphere at a heating rate of 10 °C/min. The weight loss curves were recorded. The thermograms of the PHB/PCL mixture were also investigated for comparison purposes.

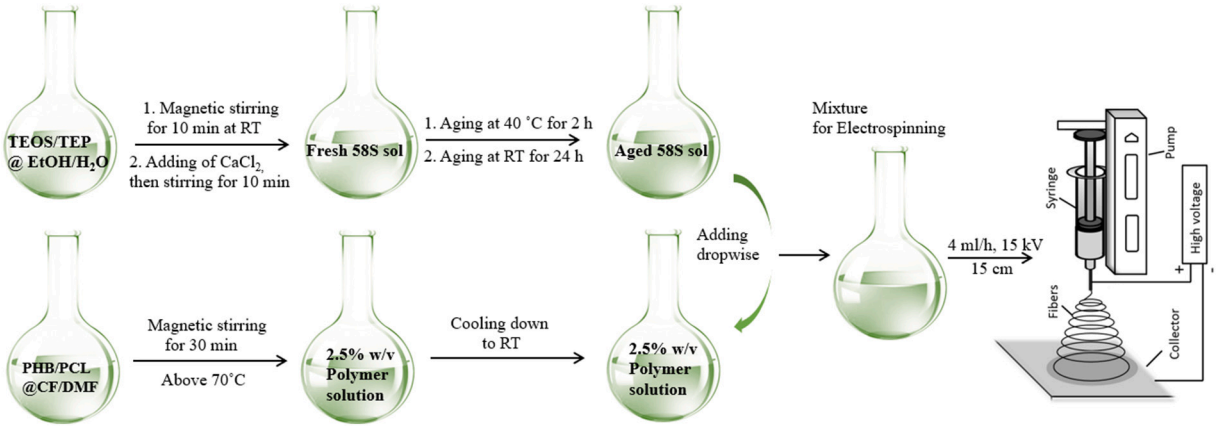

Fig. 1. Schematic illustration on the fabrication process of honeycomb-like hybrid structures.

2.4. Cellular studies

MG-63 osteoblast-like cells (MG-63 cells, Sigma-Aldrich, USA) were cultured in a Dulbecco's modification of Eagle's medium (DMEM) (HyClone, Logan, UT) with 4.5 g/L glucose, supplemented with 10% fetal bovine serum (Gibco, Invitrogen, USA), 1% nonessential amino acids, 1% L-glutamine, penicillin (100 IU/mL) and streptomycin (100 μg/mL) (all from HyClone, Logan, UT). The cells were cultured in a 95% humidified atmosphere with 5% of CO_2 at 37 °C. The medium was changed every other day. As-prepared samples were sterilized with UV-light radiation for 1 h before cell culture.

2.4.1. Cell viability

To investigate the biocompatibility of the scaffolds, MG-63 cells were seeded onto the samples in 96-well plates at a density of 1×10^4 cells per well, and the AlamarBlue® Cell Viability Assay (Thermo Fisher Scientific, USA) was utilized. After cell culture for 1 and 3 days, the culture medium was removed, and samples were incubated in fresh Hanks' balanced salt solution (HBSS) containing 10 vol% AlamarBlue® solutions at 37 °C in 5% CO_2 for another 4 h. When the medium color changed from blue to light pink, the luminescence of the reacted medium (100 μL) was measured using a Varioskan Flash plate reader (Thermo Fisher Scientific, USA), which indicated the live cell numbers proportionally. The experiments were repeated in triplicate.

2.4.2. Cell proliferation and infiltration

To evaluate the cell proliferation, MG-63 cells were cultured onto the samples in 48-well plates at a density of 2×10^4 cells per well for 3 and 7 days. The fibrous samples were kept at the bottom of the wells using small glass cylinder tubes. At each time point, cell-seeded samples were fixed in 2.5% glutaraldehyde for 30 min, rinsed with phosphate-buffered saline (PBS) several times, and then dehydrated through a concentration-graded ethanol at 30, 50, 70, 80, 90, and 100% for 15 min each. The dehydrated samples were sputter-coated with platinum before SEM observation (Quanta 250 FEG, FEI, USA).

For a deeper insight into the cell infiltration in the scaffolds, MG-63 cells were seeded onto the samples in 48-well plates at a density of 2×10^4 cells per well, and then cultivated in the medium for 3 and 7 days. At each time point, the samples were fixed with 4% paraformaldehyde for 10 min, and then washed with PBS three times. Before observation by confocal laser scanning microscopy (CLSM, Leica TCS SP5 II HCS A, Germany), the cells were permeabilized with 0.1% Triton X-100 for 5 min, rinsed with PBS and blocked with 1% bovine serum albumin solution for 20 min. Afterwards, the cytoskeletons were stained with Alexa Fluor® 488 phalloidin for 20 min and nuclei were stained using 4′,6-diamidino-2-phenylindole (DAPI) for 5 min.

2.5. Statistical analysis

Cell viability data were expressed as average ± standard deviation (SD). A one-way analysis of variance (ANOVA) followed by the Bonferroni *post hoc* test was used to analyze the data. The analysis was carried out using OriginPro 9.0 software (OriginLab Corporation, USA) and the level of significance was set at the probabilities of $*p < 0.05$, $**p < 0.01$ and $***p < 0.001$.

3. Results analysis

3.1. Preparations and physicochemical features of the self-assembled scaffolds

A semi-liquid state of charged nanofibers when landing on the substrate was considered the crucial condition to form the self-assembled honeycomb-like structure during electrospinning [10]. Therefore, all parameters influencing the system volatility, such as composition, concentration, voltage and working distance, may affect the initiation of the SAES process [9–12]. Solution concentration is considered the key player among those parameters and can be feasibly adjusted to tune the volatility of the hybrid system [10,25]. Only droplets or non-woven fibermats may form if the solution concentration is too low or too high [10]. Thus, to initiate the SAES process for the former optimized PHB/PCL/58S hybrid system, we firstly reduced the solution concentration from 5% w/v to 2.5% w/v while other operation parameters were applied as same to 5%P5B1 [23].

It turned out that a hybrid scaffold with honeycomb-like architectures was indeed successfully prepared through this one-step SAES process. The morphology of the as-prepared 2.5%P5B1 scaffold is shown in Fig. 2(a–c), which is characterized by a well-organized honeycomb-like architecture with a gradient porous layout. The scaffold is constituted by uniform nanofibers at around 370 ± 77 nm that self-assemble into polygonal pores between 200 μm to 1000 μm (Fig. 3(a–c)). Moreover, in addition to the random nanofibers spanning the large pores, the in-depth walls of the pore channels are constructed by uniaxially aligned nanofibers adhering to each other, indicating delayed solvent evaporation during the self-organization of nanofibers. Overall, the pore size of this honeycomb-like structure has a bimodal distribution (Fig. 3(a–b)). Surrounded by in-depth walls, the large pores with an average size of around 512 μm are conducive to cell infiltration; while the small pores of few micrometers, formed by random fibers spanning the walls, are advantageous for cell adhesion and migration. It is apparent that the reduced solution concentration from 5% w/v to 2.5% w/v not only induced the drastic reduction of fiber diameters but indeed promoted the self-assembly process of electro-charged nanofibers. The competitive actions of surface tension and electrostatic repulsion among the charged

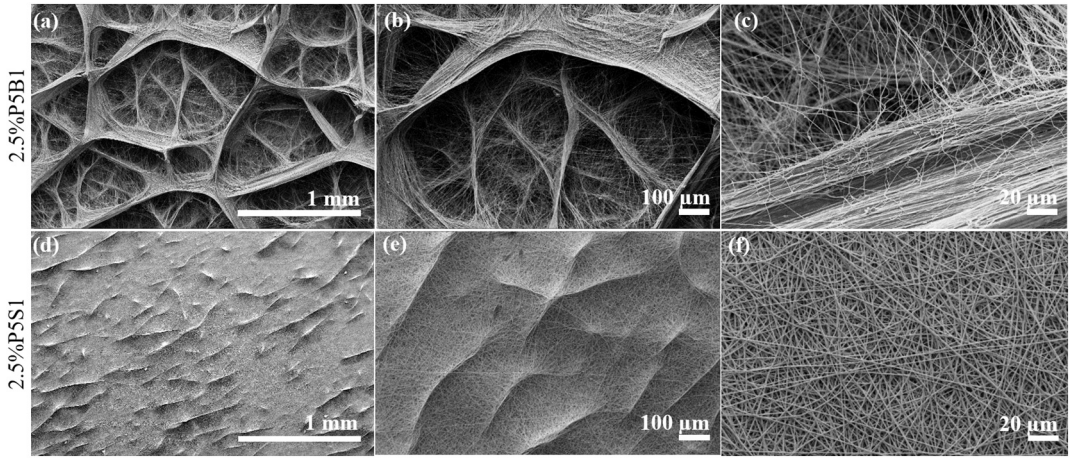

Fig. 2. Morphology characterizations of the as-prepared honeycomb-like structure 2.5%P5B1 (a–c) and non-woven fibermats 2.5%P5S1 (d–f).

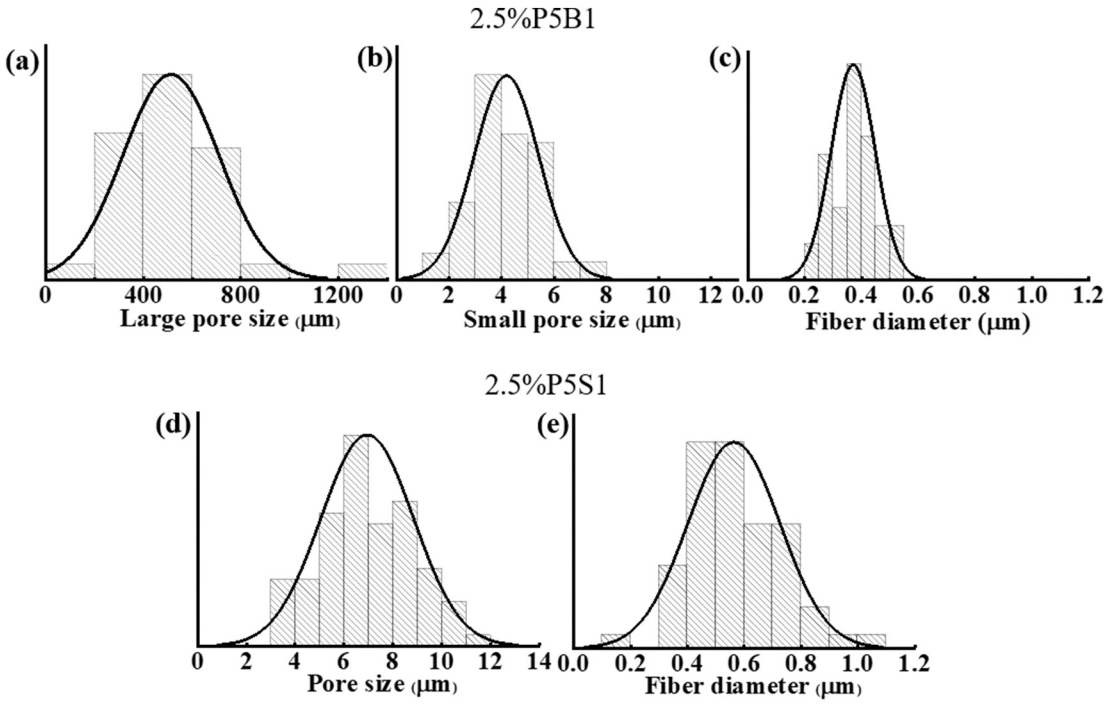

Fig. 3. Large and small pore size distribution of 2.5%P5B1 is shown in (a) and (b), respectively; pore size distribution of 2.5%P5S1 is shown in (d); fiber diameter distributions of 2.5%P5B1 and 2.5%P5S1 are shown in (c) and (e), respectively.

semi-liquid fibers are believed to drive the self-assembly process [10]. Specifically, under a high electric field, the surface tension drives the half-wet nanofibers to self-align and merge together to form the pore wall, whereas, until a critical point, the accumulated electrostatic repulsion forces among the highly charged wet nanofibers will divert the incoming nanofibers to form neighboring pores.

To find out if solution concentration was the only factor enabling the self-assembly process in this system, a PHB/PCL/sol-gel silica hybrid scaffold from another formerly optimized hybrid system was also prepared at the same conditions when the solution concentration was reduced to 2.5% w/v (2.5%P5S1) [24]. As shown in Fig. 2(d–f), unlike the honeycomb-like structures with large pores, this scaffold is mainly composed of non-woven fibers of 560 nm in average diameter and typical small pores of few micrometers (Fig. 3(d–e)), with randomly distributed ridges. No conglutination behavior was observed between the separate nanofibers.

To investigate whether and how the addition of different inorganic components affected the self-assembly process, FTIR was conducted on both samples (Fig. 4(a)). Since a thorough discussion on the spectrum of PHB/PCL/58S non-woven structures has been conducted in our previous study [23,24], only the essential bands that may cause the structural variations were discussed here. Sol-gel derived 58S bioactive glass and sol-gel derived silica were also characterized for comparison purposes. Due to the low incorporation ratio and the overlapped spectra, not all bands of the inorganic components can be identified in the final scaffolds. Nevertheless, the detection of changes in the band of 3400 cm^{-1}, 1632 cm^{-1}, and the overall intensity reduction around 1200–1000 cm^{-1} and 750–525 cm^{-1} all indicated the successful incorporation of the inorganic components. It is worth noting that the broad band at around 3400 cm^{-1} only appears in 2.5%P5B1 and not in 2.5%P5S1, indicating that the amount of residue -OH of 58S-containing scaffolds is higher than that of the silica-containing non-woven structure. The high retention of -OH groups may also contribute to the retarded solvent evaporation, and thus, further facilitates the self-assembly process. Therefore,

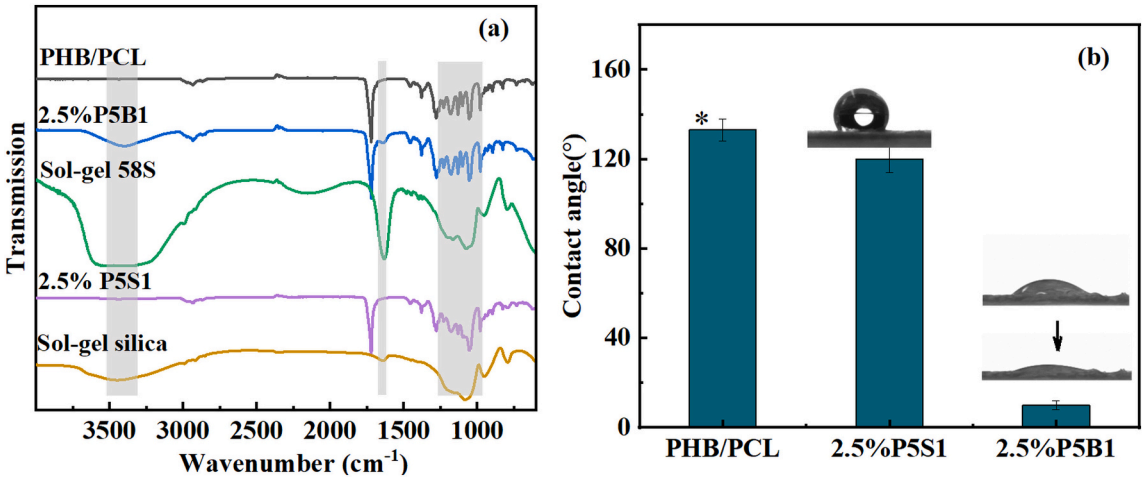

Fig. 4. (a) FTIR spectra and (b) contact angle measurements on the as-prepared honeycomb-like structures 2.5%P5B1 and non-woven fibrous structures 2.5%P5S1 (* represents the reference from previous study) [23].

it can be concluded that both the reduced solution concentration and the addition of 58S bioactive glass sol caused insufficient solvent evaporation, which resulted in the self-alignment of half-liquid fibers and generation of the honeycomb-like structures.

The wettability of the structures was investigated through water contact angle measurements. As shown in Fig. 4(b), in comparison to the hydrophobic PHB/PCL scaffolds, the incorporation of both sol-gel derived 58S and silica can improve the hydrophilicity. Especially the honeycomb-like structure with 58S addition showed super-hydrophilicity with a decreasing contact angle from around 30° to 0° within few seconds. This result is consisting with our former study on PHB/PCL/58S hybrid scaffolds with non-woven structures. Both the high retention of -OH groups and the large pore size were considered contributing to the superhydrophilicity of the 58S-containing honeycomb-like structures.

More characterization to understand the thermal properties of the obtained structures were investigated through DSC and TG analysis (Fig. 5(a–b)). As shown in Fig. 5(a), both melting peaks of PHB and PCL were detected in all samples, presenting the semi-crystalline nature of PHB and PCL. However, the melting points of PHB and PCL were slightly decreased in the honeycomb-like structure 2.5%P5B1 in comparison to other samples, indicating a stronger inhibition effect of sol-gel 58S on polymer crystallization during electrospinning. Additionally, the extra endothermic peak at around 100–110 °C on the curve of 2.5%P5B1 was possibly caused by the moisture evaporation of sol-gel 58S, as reported by Kargozar et al. [26]. TG analysis in Fig. 5(b) presents the weight loss during the heating from room temperature to 600 °C. There was almost no weight loss until 200 °C for the silica-containing sample and pure polymer mixture, whereas around 4.6% weight loss before 200 °C caused by the 58S sol degradation was recorded in the 58S-containing sample 2.5%P5B1. Both DSC and TG analysis indicated residual moisture in the 58S-containing samples, which is consisting with the FTIR results.

3.2. Cell-scaffolds interactions

To evaluate the cell-scaffold interactions, a model cell line, *i.e.*, MG-63 cells were cultured on both samples for 1, 3, and 7 days. Each of the constituting components of the scaffolds, *e.g.*, PHB, PCL, and sol-gel derived silica and 58S showed well-preserved biocompatibility in previous studies regarding non-woven fibermats [23]. Nevertheless, uncertainty about whether the hierarchical structure will affect the cell viability/proliferation remains. The MG-63 cells viability was evaluated after cultivation for 1 and 3 days to assess the biocompatibility of the as-prepared hierarchical structure. As shown in Fig. 6, both scaffolds showed comparable cell viability to the control group (tissue culture plate). There was no significant difference between the two structures and the control, indicating good biocompatibility of the electrospun fibermats and honeycomb-like structure.

Cell proliferation on both scaffolds was investigated using the SEM

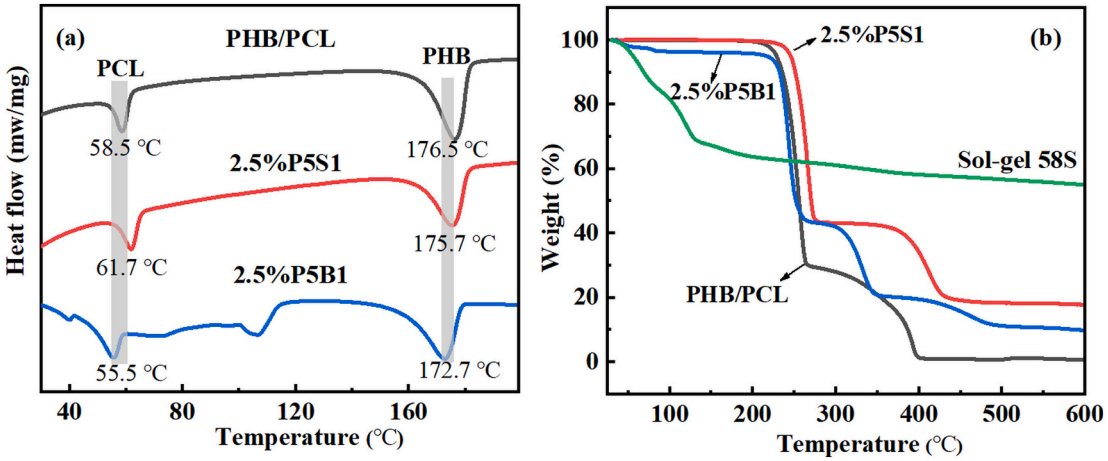

Fig. 5. (a) DSC thermograms and (b) TG analysis of honeycomb-like structures 2.5%P5B1 and non-woven fibrous structures 2.5%P5S1.

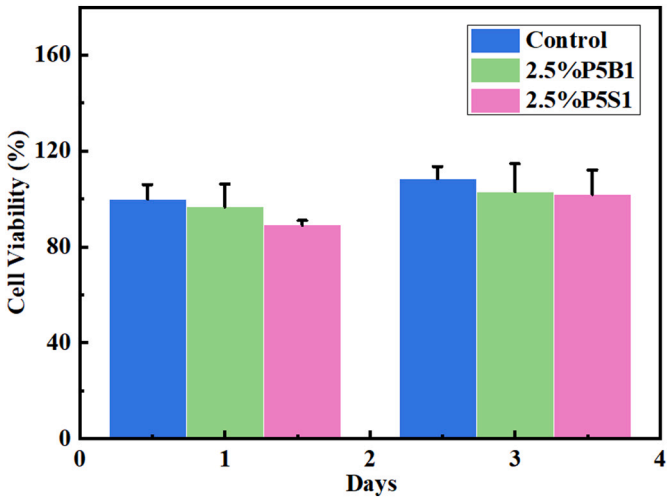

Fig. 6. Cell viability of MG-63 cells on 2.5%P5B1 and 2.5%P5S1 scaffolds for 1 and 3 days at 37 °C using AlamarBlue® Cell Viability Assay.

after cell cultivation for 3 and 7 days. As shown in Fig. 7, well-attached cells grew mostly along the guidance of porous structure. When cells were incubated on 2.5%P5B1 scaffolds with a honeycomb-like structure, they not only attached to the upper layer and comb-wall, but also grew and infiltrated into the bottom layer of the large pores (Fig. 7(a–c)). While on 2.5%P5S1 scaffolds with pore sizes of a few micrometers, cells merely spread across the surface layer of scaffolds (Fig. 7(f–h)). Intensively proliferated cells fully occupied the top surface of both scaffolds after 7 days of culture. The walls of the honeycomb-like structure are still clearly visible through the cell colonization (Fig. 7(d, e)), whereas cracks appear on non-woven fibrous scaffolds due to the thickening of cell layers and drying process for SEM (Fig. 7(i, j)). Overall, compared to the non-woven scaffolds, honeycomb-like structures with both large and small pores regulated the cell attachment and proliferation along the pore patterns to some extent.

There was evidence that cells can conveniently grow into the bottom of large pores in a honeycomb-like structure, though it was still unclear how deep the cells can penetrate the whole scaffolds. Confocal microscopy was further utilized to investigate the spatial distribution of cells. The cell nuclei and cytoskeletons were stained to display the spatial organization of cells after cultivation for 3 and 7 days. As shown in Fig. 8 (a), after 3 days, cell distribution surrounding a large pore in the range of 300–400 μm was observed on scaffold 2.5%P5B1. Meanwhile, stained nuclei were also spotted on the inner area of the pore, indicating cell distribution within the pores. Random cell distribution was noticed on scaffolds 2.5%P5S1 (Fig. 8(e)). Cells proliferated extensively on both scaffolds after cultivation for 7 days, and the highly accelerated cell numbers allow a proper overall analysis of cellular spatial distribution. Thus, a set of 3D-reconstructed images based on the Z-stacks of confocal imaging are shown in Fig. 8(b, c) for 2.5%P5B1, and Fig. 8(f, g) for 2.5% P5S1. The honeycomb-like pattern of 2.5%P5B1 was still identified in Fig. 8(b), while cell distribution with a random pattern, probably due to the cracks (Fig. 7(j)), is shown in Fig. 8(f) for 2.5%P5S1 scaffolds. 3D reconstructed images along the thickness direction (Z-axis) are shown in Fig. 8(c, g). It seems that the cell infiltration within honeycomb-like structures reached 100–200 μm, while the cells on non-woven structures may stay only on the surface, *i.e.*, around tens of micrometers. Furthermore, the Z-stack images of one spot from each sample, indicating the cell location in different layers along the Z-axis, are shown in Fig. 8(d, h). Specifically, the fluorescence signal can be detected until 150 μm depth in the honeycomb-like structure and only around 30 μm in the non-woven structure.

4. Discussion

In our previous study, a series of PHB/PCL/58S hybrid scaffolds with non-woven structures were prepared through combinational sol-gel method and electrospinning technique, aiming to mimic the ECM structurally and compositionally. The physicochemical alterations induced by the incorporation of 58S were thoroughly investigated through topographical characterizations, mechanical testing, wettability measurements, and thermal analysis. Moreover, the cell culture studies demonstrated that the addition of sol-gel derived 58S components can drastically improve the wettability and also enhance the osteogenicity of the polymer scaffolds [23]. Nevertheless, the obtained structures represented the ordinary layer-by-layer stacked fibrous structure with micropores, which highly restrict the cell infiltration, especially in the early stage before the scaffolds degradation [8,27].

Herein, a self-assembled PHB/PCL/58S scaffold with honeycomb-like architectures was fabricated based on our pre-optimized hybrid system by reducing the solution concentration. The reduction of the solution concentration was assumed to cause the delayed solvent evaporation and enable following initiation of the self-assembly process, which was proved a general phenomenon for electrospun honeycomb-like structures [10,28]. However, when the solution concentration was reduced for another pre-optimized PHB/PCL/sol-gel silica hybrid system, only non-woven structures can be prepared at the same conditions. The FTIR measurements, DSC thermographs and TG analysis between the two hybrid systems indicated that high -OH retention appeared only on the PHB/PCL/58S honeycomb-like structures, which is hypothesized to also contribute to the retarded solvent evaporation in the obtained honeycomb-like structures. The self-assembled pores consisting of both

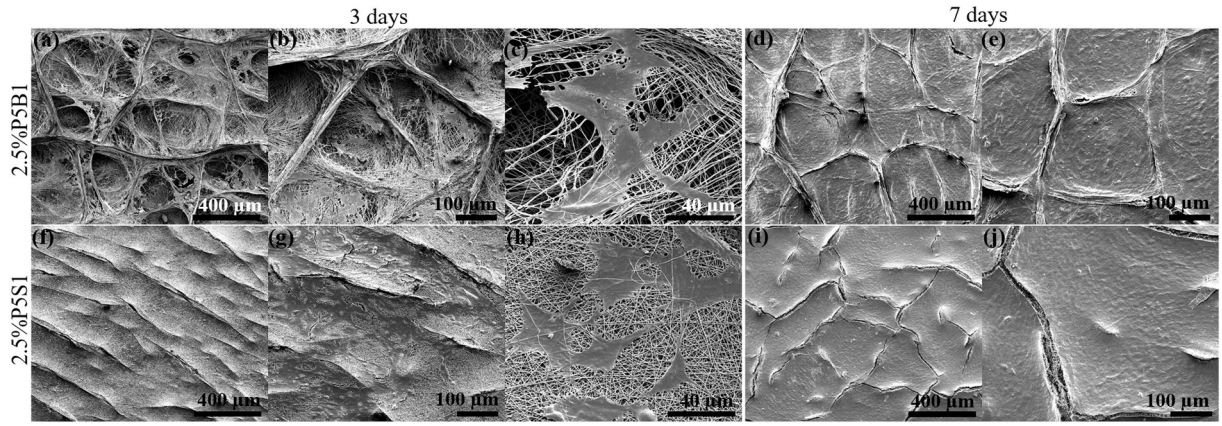

Fig. 7. SEM images of MG-63 cell proliferation on 2.5%P5B1 scaffolds (a, b, c) for 3 days and (d, e) for 7 days, and on 2.5%P5S1 scaffolds (f, g, h) for 3 days and (i, j) for 7 days.

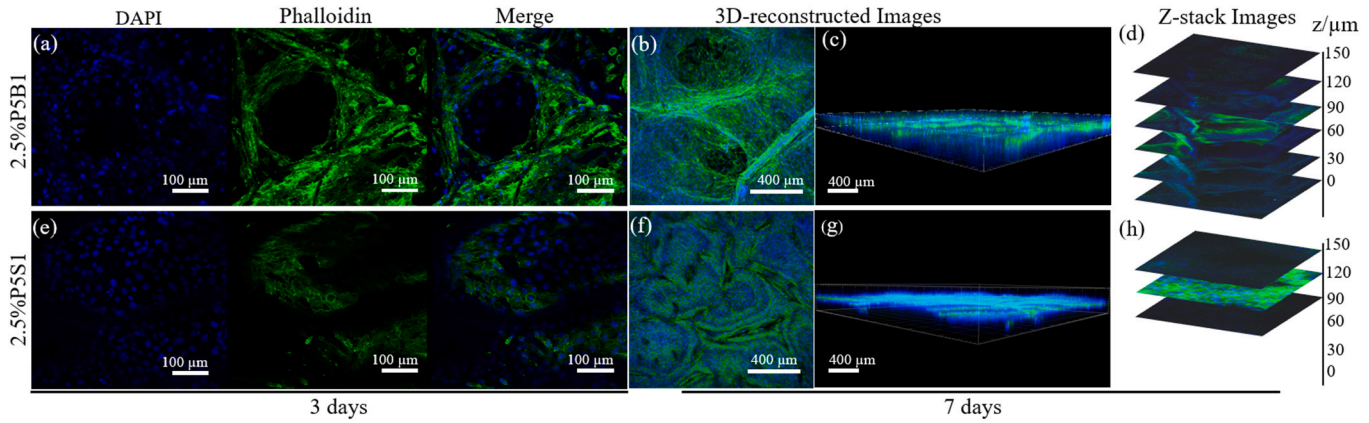

Fig. 8. Confocal images of MG-63 cells when cultivated on 2.5%P5B1 scaffolds (a) for 3 days and (b, c, d) for 7 days, and on 2.5%P5S1 scaffolds (e) for 3 days and (f, g, h) for 7 days; (b, c, f, g) are the 3D-reconstructed images of cell distribution on both samples after cultivation for 7 days; (d, h) are the in-depth Z-stack images of cells cultivation on both samples for 7 days.

micropores at around few micrometers and mesopores up to several hundreds of micrometers were considered beneficial for improved cellular interactions [13,28–29]. Cell culture studies up to 7 days on both honeycomb-like and non-woven structures suggested that both systems showed comparable biocompatibility to MG-63 cells evidenced by the cell viability and cell proliferation studies. However, the cell spatial organization was highly regulated by the honeycomb-like patterns and the cell infiltration was around 5 times deeper than the nonwove structures.

Multiple parameters can influence the complex interplays between cells and scaffolds, including but not limited to the materials compositions, topography cues, and surface wettability [30]. Since this is extended research to our previous study, only the key novelty compared to the former research, *i.e.*, the structural variation, was highlighted and discussed in the present study. The ideal comparison groups should be PHB/PCL/58S hybrid scaffolds with honeycomb-like structures and nonwoven structures at a similar fiber diameter range. However, in our fixed PHB/PCL/58S hybrid system at a low solution concentration (2.5% w/v), it is not possible to prepare a non-woven structure under all conditions. The pore size and shape of the self-assembled structures in electrospinning may vary when the parameters, *e.g.* voltage and working distances, were adjusted [9]. Beads, beads on fibers, or irregular pores can be formed from a fixed solution at low concentration [11]. Thus, a similar hybrid PHB/PCL/sol-gel silica scaffold with non-woven structures prepared at the same operational conditions was applied here to evaluate the cell response to the structural variations. Despite the differences in the scaffolds' composition and wettability, cell viability studies showed comparable biocompatibility between the two systems. Cell proliferation after 7 days showed that MG-63 cells fully occupied the top surface of both scaffolds, suggesting comparable cell proliferation environments provided by the two scaffolds. The significant difference in cell responses to the two systems was highlighted by the cell infiltration and cell spatial organization, which we hypothesize can prove the benefits from the obtained honeycomb-like structures.

For successful tissue regeneration, scaffolds are expected to not only mimic the chemical components of natural tissues, but also to resemble the physical structure of natural ECM as closely as possible. Specifically, the topography, pore size, and curvature of scaffolds can all affect the cell behaviors at different levels [31]. For instance, Graziano et al. proposed that cells cultured on the scaffolds featuring concave textured surfaces exhibited improved cell-scaffold interactions and accelerated vascularization [32]. Taking bone remolding process as an example, osteons/hemi-osteons, characterized with circular/semicircular cavities and grooves ranging around a few hundreds of microns, facilitate the recruitment of osteoblasts to form neo-bone [33–35]. To mimic the osteon/hemi-osteon structure, scaffolds with circular or semi-circular cavities with concave curvatures have been prepared and investigated for promoted cell-scaffolds interactions [35–37]. Among them, honeycomb-like scaffolds with concave pores are considered ideal options to mimic the hemi-osteons. The interconnectivity of voids available in the structures is ideal for tissue ingrowth, exchange of nutrients and the metabolism of waste without structural deformation [38]. Takabatake et al. proved that a tricalcium phosphate scaffold with the honeycomb-like arrangement was a suitable scaffold for promoting bone tissue formation [39]. Nedjari et al. prepared by using a micro-patterned honeycomb collector, a honeycomb-like electrospun scaffold that mimics the hemi-osteon-like cavities to control the osteoblast spatial organization [40]. Garcia et al. developed an electrospun PCL/hydroxyapatite honeycomb structure using a honeycomb collector, aiming to provide cells with a 3D environment [41]. Their study showed that high colonization surface of the honeycomb structure guided the migration of the cells throughout the cavities and the ridge of the honeycomb-like pores, which is consistent with our study here.

As indicated above, most reported organic-inorganic scaffolds with honeycomb-like structures were collected on a honeycomb template, which required an added manufacturing technique, *e.g.*, photolithography [41]. Our study is the first report on a one-step approach without additional processing to endow electrospun organic-inorganic hybrid scaffolds with the honeycomb-like structure. This method is considered a cost-effective and straightforward approach to fabricate bioactive scaffolds with honeycomb-like architecture in comparison to the template approach. Non-woven PHB/PCL/58S hybrid fibermats showed high osteogenic potential in previous study, owing to the addition of sol-gel derived bioactive glass [23]. Thus, we can expect that our newly prepared honeycomb-like hybrid scaffold can integrate the enhanced osteogenic potential and the improved cell-scaffold interactions, resulting in maximized tissue ingrowth.

5. Conclusions

Overall, we firstly prepared an organic-inorganic hybrid scaffold with honeycomb-like structures through the self-assembly-driven electrospinning process. From the comparative studies, it is concluded that both the low solution concentration and the addition of sol-gel derived 58S with high -OH retention were assumed to cause the retarded solvent evaporation, which enabled the semi-liquid fibers to self-align and adhere to form the wall of the honeycomb-like structures. MG-63 osteoblast-like cells showed extensively improved cell ingrowth and infiltration into the honeycomb-like scaffold, and the spatial distribution of the cells was regulated by the honeycomb-like pattern. The high infiltration of the cells ensures sufficient space for cell proliferation, and the large pores ranging around a few hundreds of micrometers may allow

the efficient exchange of cellular metabolism and nutrition, making the hybrid scaffolds a prime candidate for tissue regeneration. As a proof-of-concept, this study focuses on the investigation of morphology, chemical composition and cell-material interactions in the spatial dimension. Deeper insights into the performances of the scaffolds, such as the osteogenicity and angiogenesity, will be further investigated in up-coming studies.

CRediT authorship contribution statement

Yaping Ding: Conceptualization, Investigation, Writing - Original draft preparation.
Wei Li: Writing - Review & editing.
Dirk W. Schubert: Resources, Writing - Review & editing.
Aldo R. Boccaccini: Resources, Writing - Review & editing.
Judith A. Roether: Supervision, Writing - Review & editing.
Hélder A. Santos: Supervision, Resources, Funding acquisition, Writing - Review & editing.

Declaration of competing interest

Authors declare no conflicts of interest.

Acknowledgements

Dr. Y.P. Ding acknowledges financial support from Orion Research Foundation and Finnish Cultural Foundation. Prof. H.A. Santos acknowledges financial support from HiLIFE Research Funds, Academy of Finland (grant no. 331151) and the Sigrid Jusélius Foundation.

References

[1] R. Langer, J.P. Vacanti, Tissue engineering, Science 260 (5110) (1993) 920.
[2] P. Zhao, H. Gu, H. Mi, C. Rao, J. Fu, L.-s Turng, Fabrication of scaffolds in tissue engineering: a review, Front. Mech. Eng. 13 (1) (2018) 107–119.
[3] A. Khademhosseini, R. Langer, A decade of progress in tissue engineering, Nat. Protoc. 11 (10) (2016) 1775–1781.
[4] S. Chen, R. Li, X. Li, J. Xie, Electrospinning: an enabling nanotechnology platform for drug delivery and regenerative medicine, Adv. Drug Deliv. Rev. 132 (2018) 188–213.
[5] Y. Ding, W. Li, F. Zhang, Z. Liu, N. Zanjanizadeh Ezazi, D. Liu, H.A. Santos, Electrospun fibrous architectures for drug delivery, tissue engineering and cancer therapy, Adv. Funct. Mater. 29 (2) (2019), 1802852.
[6] I. Jun, H.-S. Han, J.R. Edwards, H. Jeon, Electrospun fibrous scaffolds for tissue engineering: viewpoints on architecture and fabrication, Int. J. Mol. Sci. 19 (3) (2018) 745.
[7] U. Stachewicz, P.K. Szewczyk, A. Kruk, A.H. Barber, A. Czyrska-Filemonowicz, Pore shape and size dependence on cell growth into electrospun fiber scaffolds for tissue engineering: 2D and 3D analyses using SEM and FIB-SEM tomography, Mater. Sci. Eng. C 95 (2019) 397–408.
[8] J. Wu, Y. Hong, Enhancing cell infiltration of electrospun fibrous scaffolds in tissue regeneration, Bioact. Mater. 1 (1) (2016) 56–64.
[9] T. Yao, H. Chen, P. Samal, S. Giselbrecht, M.B. Baker, L. Moroni, Self-assembly of electrospun nanofibers into gradient honeycomb structures, Mater. Des. 168 (2019), 107614.
[10] G. Yan, J. Yu, Y. Qiu, X. Yi, J. Lu, X. Zhou, X. Bai, Self-assembly of electrospun polymer nanofibers: a general phenomenon generating honeycomb-patterned nanofibrous structures, Langmuir 27 (8) (2011) 4285–4289.
[11] T. Liang, S. Mahalingam, M. Edirisinghe, Creating "hotels" for cells by electrospinning honeycomb-like polymeric structures, Mater. Sci. Eng. C 33 (7) (2013) 4384–4391.
[12] T.C. Reis, I.J. Correia, A. Aguiar-Ricardo, Electrodynamic tailoring of self-assembled three-dimensional electrospun constructs, Nanoscale 5 (16) (2013) 7528–7536.
[13] T. Yao, P.A. Wieringa, H. Chen, C. Amit, P. Samal, S. Giselbrecht, M.B. Baker, L. Moroni, Fabrication of a self-assembled honeycomb nanofibrous scaffold to guide endothelial morphogenesis, Biofabrication 12 (4) (2020), 045001.
[14] Y. Liu, G. Xu, J. Wei, Q. Wu, X. Li, Cardiomyocyte coculture on layered fibrous scaffolds assembled from micropatterned electrospun mats, Mater. Sci. Eng. C 81 (2017) 500–510.
[15] C. Dai, Y. Li, W. Pan, G. Wang, R. Huang, Y. Bu, X. Liao, K. Guo, F. Gao, Three-dimensional high-porosity chitosan/honeycomb porous carbon/hydroxyapatite scaffold with enhanced osteoinductivity for bone regeneration, ACS Biomater. Sci. Eng. 6 (1) (2020) 575–586.
[16] J. George, J. Onodera, T. Miyata, Biodegradable honeycomb collagen scaffold for dermal tissue engineering, J. Biomed. Mater. Res. A 87A (4) (2008) 1103–1111.
[17] C.-C. Wang, K.-C. Yang, K.-H. Lin, C.-C. Wu, Y.-L. Liu, F.-H. Lin, I.-H. Chen, A biomimetic honeycomb-like scaffold prepared by flow-focusing technology for cartilage regeneration, Biotechnol. Bioeng. 111 (11) (2014) 2338–2348.
[18] S.H. Ralston, Bone structure and metabolism, Medicine 45 (9) (2017) 560–564.
[19] S. Nedjari, F. Awaja, G. Altankov, Three dimensional honeycomb patterned fibrinogen based nanofibers induce substantial osteogenic response of mesenchymal stem cells, Sci. Rep. 7 (1) (2017) 15947.
[20] Y. Wang, W. Cui, J. Chou, S. Wen, Y. Sun, H. Zhang, Electrospun nanosilicates-based organic/inorganic nanofibers for potential bone tissue engineering, Colloids Surf. B: Biointerfaces 172 (2018) 90–97.
[21] X. Wang, J. Chang, C. Wu, Bioactive inorganic/organic nanocomposites for wound healing, Appl. Mater. Today 11 (2018) 308–319.
[22] J. Bramhill, S. Ross, G. Ross, Bioactive nanocomposites for tissue repair and regeneration: a review, Int. J. Environ. Res. Public Health 14 (1) (2017) 66.
[23] Y. Ding, W. Li, T. Müller, D.W. Schubert, A.R. Boccaccini, Q. Yao, J.A. Roether, Electrospun polyhydroxybutyrate/poly(ε-caprolactone)/58S sol–gel bioactive glass hybrid scaffolds with highly improved osteogenic potential for bone tissue engineering, ACS Appl. Mater. Interfaces 8 (27) (2016) 17098–17108.
[24] Y. Ding, J.A. Roether, A.R. Boccaccini, D.W. Schubert, Fabrication of electrospun poly (3-hydroxybutyrate)/poly (ε-caprolactone)/silica hybrid fibermats with and without calcium addition, Eur. Polym. J. 55 (2014) 222–234.
[25] D.W. Schubert, Revealing novel power laws and quantization in electrospinning considering jet splitting—toward predicting fiber diameter and its distribution, Macromol. Theory Simul. 28 (4) (2019), 1900006.
[26] S. Kargozar, F. Baino, S. Banijamali, M. Mozafari, Synthesis and physico-chemical characterization of fluoride (F)- and silver (Ag)-substituted sol-gel mesoporous bioactive glasses, Biomed. Glas. 5 (1) (2019) 185–192.
[27] J. Hodge, C. Quint, The improvement of cell infiltration in an electrospun scaffold with multiple synthetic biodegradable polymers using sacrificial PEO microparticles, J. Biomed. Mater. Res. A 107 (9) (2019) 1954–1964.
[28] D. Ahirwal, A. Hébraud, R. Kádár, M. Wilhelm, G. Schlatter, From self-assembly of electrospun nanofibers to 3D cm thick hierarchical foams, Soft Matter 9 (11) (2013) 3164–3172.
[29] S. Bongiovanni Abel, F. Montini Ballarin, G.A. Abraham, Combination of electrospinning with other techniques for the fabrication of 3D polymeric and composite nanofibrous scaffolds with improved cellular interactions, Nanotechnology 31 (17) (2020), 172002.
[30] X. Yao, R. Peng, J. Ding, Cell–material interactions revealed via material techniques of surface patterning, Adv. Mater. 25 (37) (2013) 5257–5286.
[31] A. Denchai, D. Tartarini, E. Mele, Cellular response to surface morphology: electrospinning and computational modeling, Front. Bioeng. Biotechnol. 6 (2018) 155.
[32] A. Graziano, R. d'Aquino, M.G.C.-D. Angelis, F. De Francesco, A. Giordano, G. Laino, A. Piattelli, T. Traini, A. De Rosa, G. Papaccio, Scaffold's surface geometry significantly affects human stem cell bone tissue engineering, J. Cell. Physiol. 214 (1) (2008) 166–172.
[33] B. Chang, X. Liu, Osteon: structure, turnover and regeneration, Tissue Eng. Part B Rev. (2021), https://doi.org/10.1089/ten.TEB.2020.0322.
[34] R.F.M. van Oers, R. Ruimerman, E. Tanck, P.A.J. Hilbers, R. Huiskes, A unified theory for osteonal and hemi-osteonal remodeling, Bone 42 (2) (2008) 250–259.
[35] C.M. Bidan, K.P. Kommareddy, M. Rumpler, P. Kollmannsberger, Y.J. Bréchet, P. Fratzl, J.W. Dunlop, How linear tension converts to curvature: geometric control of bone tissue growth, PLoS One 7 (5) (2012), e36336.
[36] S. Nedjari, G. Schlatter, A. Hébraud, Thick electrospun honeycomb scaffolds with controlled pore size, Mater. Lett. 142 (2015) 180–183.
[37] Birch, M. A.; Tanaka, M.; Kirmizidis, G.; Yamamoto, S.; Shimomura, M., Microporous "honeycomb" films support enhanced bone formation in vitro. Tissue Eng. Part A 2013, 19 (17–18), 2087–2096.
[38] H. Matsuda, K. Takabatake, H. Tsujigiwa, S. Watanabe, S. Ito, H. Kawai, M. Hamada, S. Yoshida, K. Nakano, H. Nagatsuka, Effects of the geometrical structure of a honeycomb TCP on relationship between bone/cartilage formation and angiogenesis, Int. J. Med. Sci. 15 (14) (2018) 1582–1590.
[39] Takabatake, K.; Yamachika, E.; Tsujigiwa, H.; Takeda, Y.; Kimura, M.; Takagi, S.; Nagatsuka, H.; Iida, S., Effect of geometry and microstructure of honeycomb TCP scaffolds on bone regeneration. J. Biomed. Mater. Res. A 2014, 102 (9), 2952–60.
[40] S. Nedjari, S. Eap, A. Hébraud, C.R. Wittmer, N. Benkirane-Jessel, G. Schlatter, Electrospun honeycomb as nests for controlled osteoblast spatial organization, Macromol. Biosci. 14 (11) (2014) 1580–1589.
[41] Garcia Garcia, A.; Hébraud, A.; Duval, J.-L.; Wittmer, C. R.; Gaut, L.; Duprez, D.; Egles, C.; Bedoui, F.; Schlatter, G.; Legallais, C., Poly(ε-caprolactone)/hydroxyapatite 3D honeycomb scaffolds for a cellular microenvironment adapted to maxillofacial bone reconstruction. ACS Biomater. Sci. Eng. 2018, 4 (9), 3317–3326.